LAWRENCE
LIVERMORE
NATIONAL
LABORATORY

UCRL-JRNL-223876

COMPACT ACCELERATOR CONCEPT FOR PROTON THERAPY*

G. Caporaso, S. Sampayan, Y-J. Chen, J. Harris, S. Hawkins, C. Holmes, M. Krogh, S. Nelson, W. Nunnally, A. Paul, B. Poole, M. Rhodes, D. Sanders, K. Selenes, J. Sullivan, L. Wang, J. Watson

August 22, 2006

Nuclear Instruments and Methods, B

COMPACT ACCELERATOR CONCEPT FOR PROTON THERAPY*

G. Caporaso, S. Sampayan, Y-J. Chen, J. Harris, S. Hawkins, C. Holmes, M. Krogh[a], S. Nelson, W. Nunnally[b], A. Paul, B. Poole, M. Rhodes, D. Sanders, K. Selenes[c], J. Sullivan, L. Wang, and J. Watson

Lawrence Livermore National Laboratory

P.O. Box 808, L-645

Livermore, CA 94551, USA

Abstract

A new type of compact induction accelerator is under development at the Lawrence Livermore National Laboratory that promises to increase the average accelerating gradient by at least an order of magnitude over that of existing induction machines. The machine is based on the use of high gradient vacuum insulators, advanced dielectric materials and switches and is being developed as a compact flash x-ray radiography source. Research describing an extreme variant of this technology aimed at proton therapy for cancer will be presented.

PACS: 29.17.+w, 41.75.Lx

Keywords: Pulsed accelerator, proton therapy, high gradient, dielectric wall accelerator

1. Introduction

This paper describes a new concept for compact proton therapy accelerator. The concept represents an extreme variant of a high gradient accelerator that has been under development as a

compact flash x-ray radiography source [1]. The system is called the Dielectric Wall Accelerator (DWA) and employs a variety of advanced technologies to achieve high gradient. Progress towards the development of this concept is proceeding on several fronts. The key technologies for any DWA are high gradient vacuum insulators, high bulk breakdown strength dielectrics for pulse forming lines and closing switches compatible with operation at high gradient. In addition, a suitable accelerator architecture must be found.

2. DWA for Flash X-ray Radiography

Accelerators for flash x-ray radiography are typically induction linacs that operate at energies on the order of 20 MeV with beam currents of several kiloamperes and pulsewidths of tens of nanoseconds. A typical induction linac of this type is shown in Fig. 1. These electron induction accelerators have average accelerating gradients on the order of 0.3 – 0.5 MV/Meter. The structure of a typical induction linac is shown in Fig. 2. Interest in reducing the size and hence the cost of such systems has led to the development of the DWA concept.

In the typical induction cell the pulsed power is brought in from outside the cell via coaxial transmission lines. A large magnetic core is used to inductively isolate the accelerating gap from the DC short circuit current path that connects each side of the gap. These cores tend to be very large hence limiting the accelerating gradient. The cross section area of the core required follows from integrating Faraday's law around a path that encircles the DC short circuit and which passes through the gap (MKS units):

$$V\tau = A_c \Delta B. \quad (1)$$

Here, V is the voltage that can be sustained across the gap for a time τ, A_c is the cross-sectional area of the core and ΔB is the total flux swing available in the core material up to saturation.

The accelerating gap typically occupies a relatively small fraction of the axial length of the cell yet the field stress in the gap is on the order of 10 – 20 MV/Meter for pulses that are tens of nanoseconds long. Since the beam tube is a conductor an accelerating field can only occur in the gap. If we could find an insulator capable of sustaining large electric fields over an extended length then we might be able to make a cell in which the vacuum gap is replaced with this material. If pulse-forming lines could be incorporated inside the cell to feed this insulating wall a higher gradient accelerating structure might result. Such an arrangement is shown in Fig. 3. It incorporates a "high gradient insulator" (HGI) and a new version of a zero integral pulse-forming line that does not require a magnetic core to produce a net output voltage [2].

3. High Gradient Insulators

The leading candidate for the insulating or dielectric wall in the accelerator cell is the High Gradient Insulator (HGI) [3] shown in Fig. 4. Vacuum surface flashover is thought to proceed by means of a secondary electron emission avalanche in which field emitted electrons repeatedly bombard the surface of an insulator liberating additional (secondary) electrons and dislodging adsorbed gasses. The electron current ionizes the desorbed gas and eventually forms a dense plasma that shorts out the applied voltage.

The HGI is composed of standard insulating materials but the configuration is that of thin alternating layers of floating electrodes and insulators usually with periods that are less than one millimeter. The microstructure of the electric fields in the vicinity of the surface tends to sweep

secondary electrons away from the insulator resulting in a higher flashover threshold [4]. One of the features of vacuum surface flashover that applies to conventional as well as high gradient insulators is the inverse dependence of the flashover strength on the pulsewidth as is shown in Fig. 5. This fact helps to motivate the accelerator architecture for a proton therapy machine discussed in a later section.

HGI's have been tested under a variety of extreme conditions. A very early toroidal version (Kapton and stainless steel) 2 cm long by 15 cm inner diameter used as the wall of a simple diode sustained a 420 kV, 20 ns pulse with a 1 kA electron beam passing through its center (a gradient of > 20 MV/M). A more refined Rexolite and stainless steel HGI 1 cm long by 15 cm inner diameter was placed directly across the gap of an ETA-II induction cell and run at 170 kV with a 2 kA, 50 ns electron beam passing through it at 1 Hz for approximately 20,000 shots with no breakdowns. In another test a small disc sample several millimeters (Rexolite and stainless steel) in length withstood 100 MV/M pulses of 3 ns duration [5].

4. Oil Switch Development

In order to supply the dielectric wall with a tangential electric field used for acceleration some sort of pulse forming line such as the zero integral pulse forming line or other variant must be incorporated into the cell. For any type of pulse forming line a closing switch will be required to launch the pulse. In order to push the performance of pulse forming lines up to high gradient we have been using a simple self-breaking oil switch and a planar Blumlein composed of stainless steel electrodes and either Mylar or polypropylene sheet dielectrics. Using a 50 ns

pulse charging system and polypropylene dielectrics reliable operation has been obtained at a dielectric stress of > 100 MV/M for 5 ns pulses.

The entire assembly is immersed in degassed oil. The Blumlein and its charging and output waveforms are shown in Figs. 6 and 7 respectively. The next step in the development of the switch is to add a triggering electrode to allow synchronization of multiple lines.

5. SiC Photoconductive Switch Development

The ideal closing switch for this application would be capable of high gradient operation with a very long lifetime and a low on resistance. SiC photoconductive switches offer these advantages. The intrinsic bulk breakdown strength of SiC is > 250 MV/M and the switch operates in the linear regime without avalanche or current filamentation. We have built switches from A-plane SiC and tested them up to average field stresses of 27.5 MV/M. Known field enhancements at the edges of the electrodes intensified the field by an order of magnitude and led to failure of the switch above this stress level. This field enhancement will be substantially reduced in the next generation of switches. The switches are fabricated from wafers that are approximately 400 microns in thickness and measure 12 mm by 12 mm. A line focus of laser light is directed into the edge of the switch to activate it [6]. The switches are shown in Fig. 8. Typical performance data for the switch is shown in Fig. 9.

6. Castable Dielectric Materials

Ultimately we would like to use a cast solid dielectric material in the pulse forming lines to simplify the fabrication process and to reduce the cost. For radiographic applications pulses on the order of tens of nanoseconds are required to achieve the desired dose while for the proton therapy application shorter pulses are required. Since the pulsewidth from the pulse forming line is proportional to the square root of the relative dielectric constant it would be desirable to have a material whose properties can be varied for the application. We have been using a material in which high dielectric constant nano-particles are mixed into an epoxy matrix. The net dielectric constant of the material can be varied by adjusting the concentration of the nano-particles. Test samples of the material are shown in Fig. 10. For low concentrations of the nano-particles the bulk breakdown strength of the material under DC and pulsed conditions in these small samples is > 400 MV/M as can be seen in Fig. 11. In future tests we will stress larger area samples to assess the bulk breakdown strength.

7. Virtual Single Pulse Traveling Wave Accelerator for Proton Therapy

The trends of Fig. 5 suggest another possible operating mode of the DWA. The accelerator can be fabricated with a continuous HGI as the beam tube. By controlling the timing of the closing switches in the pulse forming lines a traveling excitation can be applied to the wall. The speed of this excitation can be adjusted to keep pace with a co-moving charged particle so that the particle is continually accelerated through the structure.

Because of the inverse dependence of surface flashover strength on the pulsewidth it is tempting to push operation to extremely short pulses. However, if this is attempted it will be found that the accelerating gradient on the axis will be substantially less than that along the wall.

In order to maintain a high gradient on the axis the beam pulsewidth cannot be too short. In order to evaluate this effect we can use Maxwell's equations to find the on-axis fields given the fields at the wall. Within the beam tube the electric field satisfies the equation

$$\left(\nabla^2 - \frac{\partial^2}{\partial t^2}\right) E_z = 0. \tag{2}$$

Here E_z is the axial component of the electric field. We seek a solution that has an invariant shape as it propagates. We take the field to depend only on the radial position r and on the "retarded time" variable $\tau = t - z/u$ where u is the speed of the wall excitation so that $E_z = E_z(r,\tau)$. Substituting this form into equation (2) yields

$$\left(\frac{1}{r}\frac{\partial}{\partial r}\left(r\frac{\partial}{\partial r}\right) + \frac{1}{u^2\gamma^2}\frac{\partial^2}{\partial \tau^2}\right) E_z = 0. \tag{3}$$

Here γ is the usual Lorentz factor. Equation (3) can be solved by Fourier transforming in τ to the variable ω. The solution that is finite on the axis is

$$\tilde{E}_z(r,\omega) = \tilde{E}_o(\omega)\frac{I_o\left(\frac{\omega r}{\gamma u}\right)}{I_o\left(\frac{\omega b}{\gamma u}\right)}. \tag{4}$$

The quantity I_o is the modified Bessel function of order zero and E_o is the Fourier transform of the tangential electric field at the wall. Taking the inverse of equation (4) for a variety of wall

excitation waveforms such as a Gaussian, Super Gaussian and hyperbolic secant we obtain a nearly universal curve for the peak on-axis field if we plot against the variable θ defined in Fig. 12. The criterion is essentially that the spatial width of the wall excitation must be larger than the beam tube diameter in order that the on-axis gradient be comparable to that along the wall. For beam tube radii on the order of a few cm this criterion implies that the minimum pulsewidth of the accelerator can vary from about 5 ns at the injector down to about 1 ns at the high energy end.

Note that this is an effective, or virtual traveling wave, as the HGI tube does not support such a wave as a natural transmission mode. The wave is continually forced by wall excitation and so is able to be propagated at any speed. As a consequence, this type of accelerator is capable of accelerating any charged particle.

8. Accelerator Architectures

There are several architectures for the short pulse traveling wave accelerator that appear to be viable. In addition to the zero integral pulse forming line discussed earlier, stacks of simple Blumleins enclosed in metal container, with or without a magnetic core will produce a large accelerating gradient on-axis. This occurs when the spatial width of the wall excitation is much less than the axial length of the accelerator. A simplified diagram of the accelerator employing Blumlein stacks is shown in Fig. 13.

In order to make a dramatic change in the paradigm for proton therapy we are attempting to make an accelerator so compact that it would fit in a single treatment room in a small clinic. In order to accomplish this end we are aiming at an average accelerating gradient of 100 MV/M.

With a gradient this large space charge-induced expansion of a 100 mA proton beam will be insignificant during the 25 ns transit time through the accelerator. A compact spark discharge proton source can be used along with an arrangement of several electrodes to independently control the extracted current and final spot size on each pulse. The focusing takes place in the space between the source and the entrance to the accelerator. In addition, the beam energy can be adjusted on each pulse. A diagram illustrating the concept is shown in Fig. 14.

The accelerator system can be configured in various configurations to treat patients. The accelerator can be mounted on a gantry in an isocentric configuration or it could be mounted vertically or nearly horizontally. Some of these possible configurations are shown in Figs. 15 and 16.

The repetition rate for the accelerator can be tens of Hertz and would be limited by thermal considerations in the switches.

The next steps in the development of this concept over the next year and a half are to bring the performance levels of the components and the accelerator architectures up to the point that an integrated system can achieve 100 MV/M. Once this has been achieved the next step is to demonstrate the performance of an integrated system, *a sub-scale prototype* at the 10 MeV level.

9. Acknowledgements

This work was jointly supported by the Lawrence Livermore National Laboratory and by the University of California Davis Cancer Center. The authors gratefully acknowledge the constant support and encouragement of Dr. Ralph deVere White, Director of the U.C. Davis

Cancer Center and Dr. Cherry Murray, Deputy Director for Science and Technology at the Lawrence Livermore National Laboratory.

- Patents Pending. This work was supported under the auspices of the US Department of Energy, the University of California, Lawrence Livermore National Laboratory under Contract No. W-7405-Eng-48.

[a]University of Missouri, Rolla

[b]University of Missouri, Columbia

[c]TPL Corporation, Albuquerque, NM

References

[1] G. Caporaso, "New Trends in Induction Accelerator Technology", Proc. Int. Wkshp. Recent Progress in Induction Linacs, Tsukuba, Japan, 2003.

[2] M. Rhodes,"Ferrite-Free Stacked Blumlein Pulse Generator for Compact Induction Linacs", in Proc. IEEE. International Pulsed Power Conf., (2005).

[3] S. Sampayan, et. al., IEEE Trans. Diel. and Elec. Ins. 7 (3) pg. 334 (2000).

[4] J. Leopold, et. al., IEEE Trans. Diel. and Elec. Ins. 12, (3) pg. 530 (2005).

[5] W. Nunnally, et. al., Proc. 14th IEEE Int. Pulsed Power Conf. PPC-2003, pg. 301 (2003).

[6] J. Sullivan and J. Stanley, "6H-SiC Photoconductive Switches Triggered Below Bandgap Wavelengths", in Proc. 27 Int. Power Modulator Symposium and 2006 High Voltage Wkshp, Washington, D.C. 2006

Fig. 1. A typical induction linac used for flash x-ray radiography. The FXR is located at Lawrence Livermore National Laboratory's site 300. The energy of the machine is approximately 18 MeV. These machines have average accelerating gradients less than 1 MV/Meter.

Fig. 2. A schematic of a typical induction linac showing three induction cells. The majority of the cell volume is taken up by a ferromagnetic (or ferrimagnetic) core (the shaded material).

Fig. 3. A high gradient accelerator cell employing a high gradient insulator as the dielectric wall along with a new zero integral pulse forming line.

Fig. 4. Schematic of a conventional vacuum insulator (left) and an HGI (right). The HGI consists of alternating thin layers of floating conductors and insulators usually with a sub-millimeter period. The microstructure of the electric fields near the surface can provide a net force which sweeps secondary electrons away from the surface so that they cannot cause a breakdown.

Fig. 5. Variation of the surface flashover threshold with pulsewidth for both conventional insulators (shown in blue) and hgi's (shown in purple). HGI's perform 2x – 5x better than conventional insulators.

Fig. 6. Closeup of the switch end of the 5 ns test Blumlein showing the Mylar dielectric sheets. The entire line is submerged in degassed oil to suppress edge breakdown.

Fig. 7. Typical charging and output waveforms are shown. The charging pulse is shown in Blue and is some 60 ns long. Data from two different Blumlein output monitors is shown. The yellow trace is from a calibrated resistive monitor with relatively poor frequency response that shows the correct output amplitude while the cyan trace is from a non-calibrated capacitive probe that has excellent frequency response.

Fig. 8. SiC photoconductive switches are shown. Each wafer is about 400 microns thick and measures 12 mm by 12 mm. The switches operated up to 11 kV before breaking at the edges of the electrodes where the field was enhanced by a factor of ten over the average.

Fig. 9. Performance data is shown for the switch operated at 4 kV in air. Operation at higher voltages required immersion in oil to prevent surface flashover around the edge of the switch.

Fig. 10. Cast dielectric samples with both low (left) and high (right) concentrations of nano-particles.

Fig. 11. Pulsed test breakdown data for the low dielectric constant samples shown in Fig. 10.

Fig. 12. The inversion of equation (4) for different assumed temporal field profiles at the wall yields a nearly universal curve shown above for three different assumed profiles.

Fig. 13. Simplified schematic of the short pulse accelerator architecture. It employs two stacks of simple Blumleins and can produce a high on-axis gradient with or without a magnetic core if the spatial width of the wall excitation is short compared to the axial length of the accelerator.

Fig. 14. An illustration of the accelerator system. Electrodes located between the source and accelerator control can be used to independently control the extracted current and the beam diameter at the patient on each pulse. Focusing is accomplished using electric fields between the source and the accelerator entrance.

Fig. 15. Horizontal mount for the treatment system.

Fig. 16. Isocentric option for mounting the accelerator.

Fig. 1.

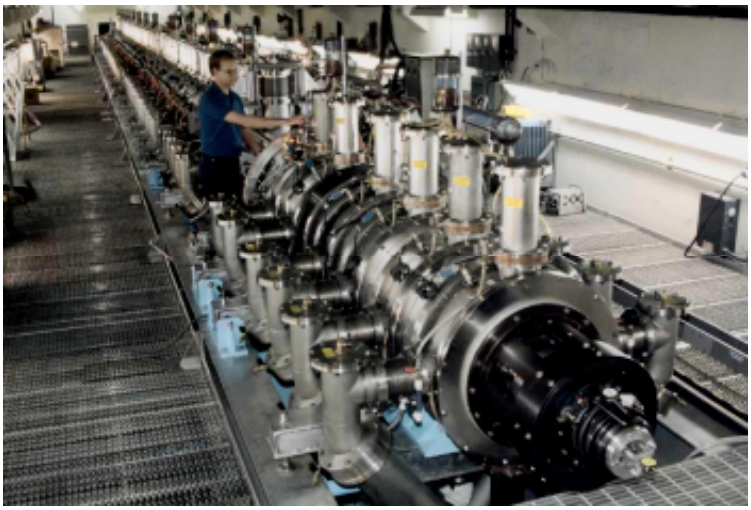

Fig. 2.

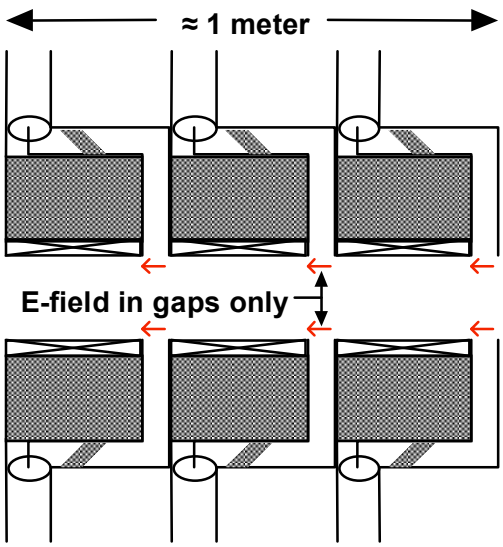

Fig. 3.

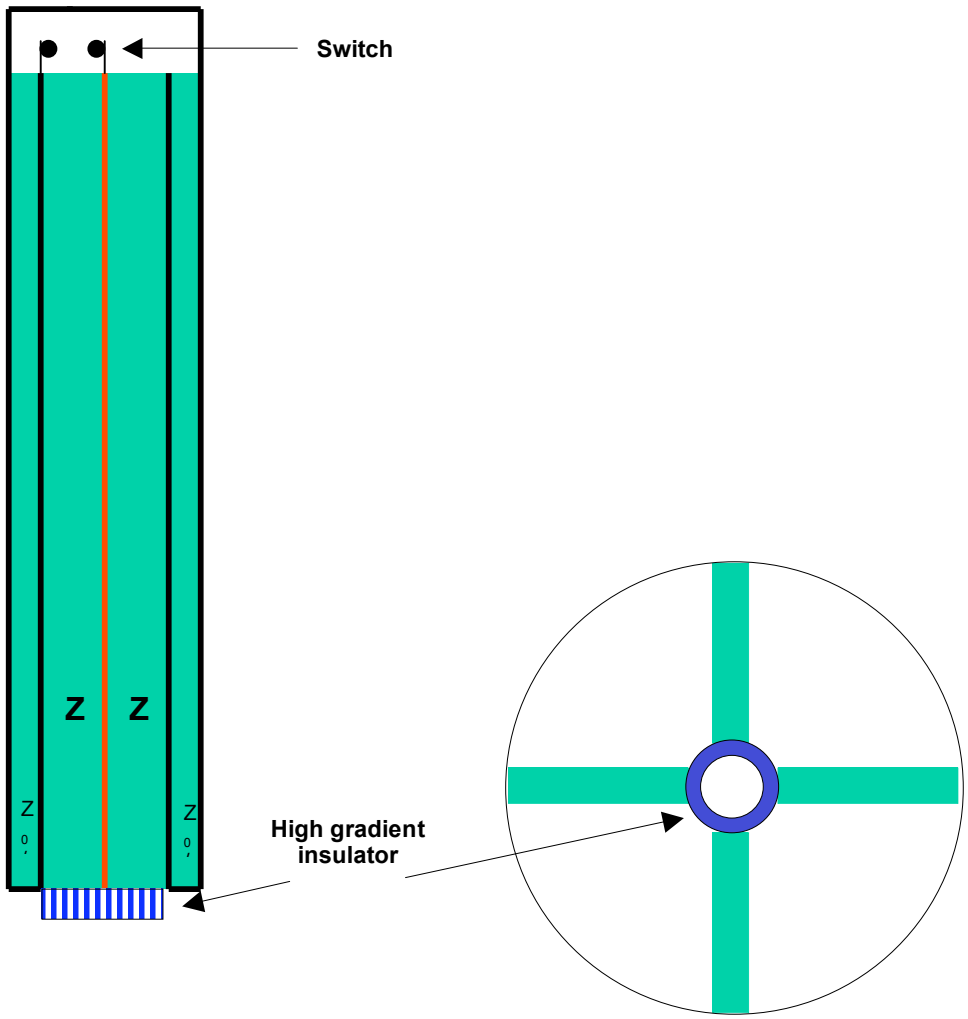

Fig. 4.

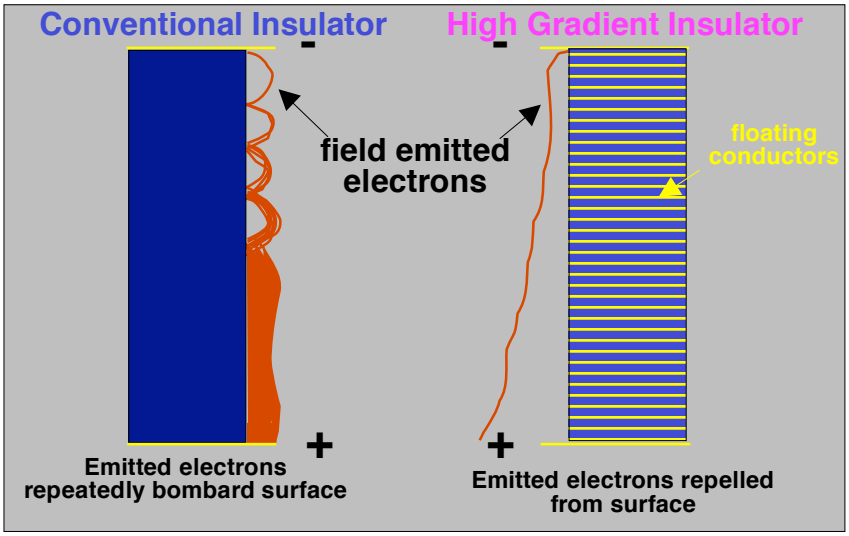
Conventional Insulator
High Gradient Insulator
field emitted electrons
floating conductors
Emitted electrons repeatedly bombard surface
Emitted electrons repelled from surface

Fig. 5.

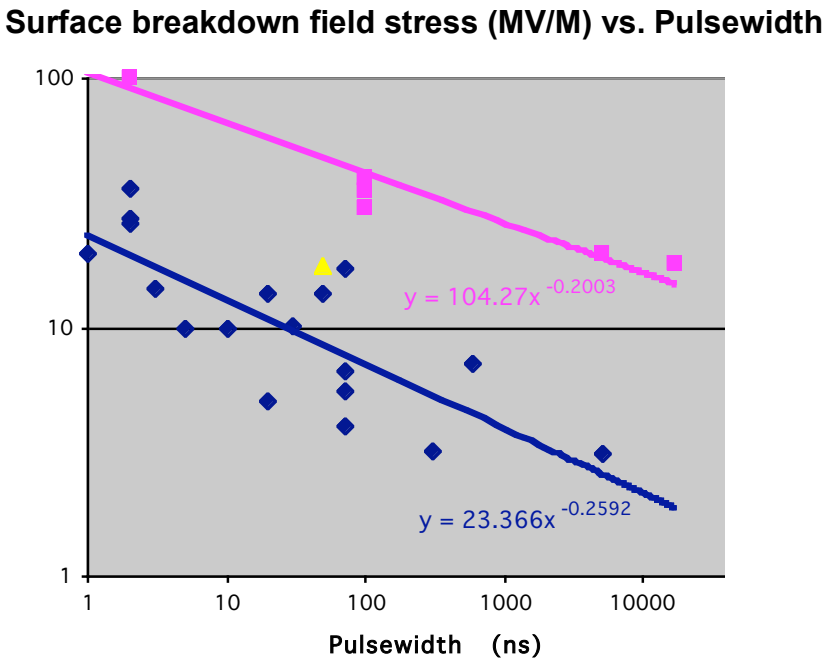
Surface breakdown field stress (MV/M) vs. Pulsewidth
100
10
1
y = 104.27x -0.2003
y = 23.366x -0.2592
1
10
100
1000
10000
Pulsewidth (ns)

Fig. 6.

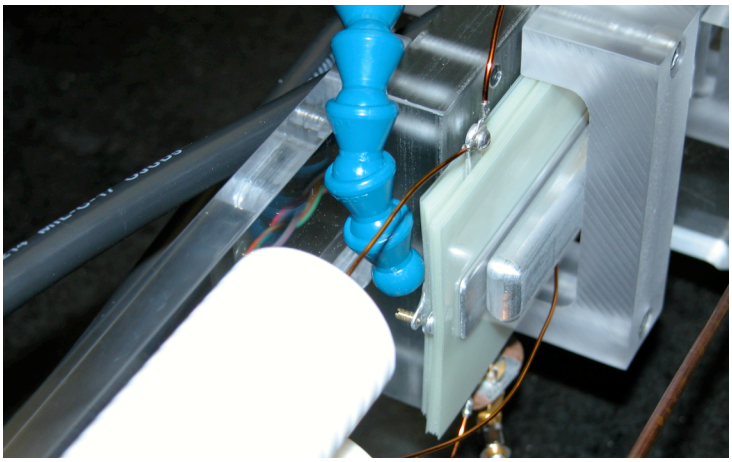

Fig. 7.

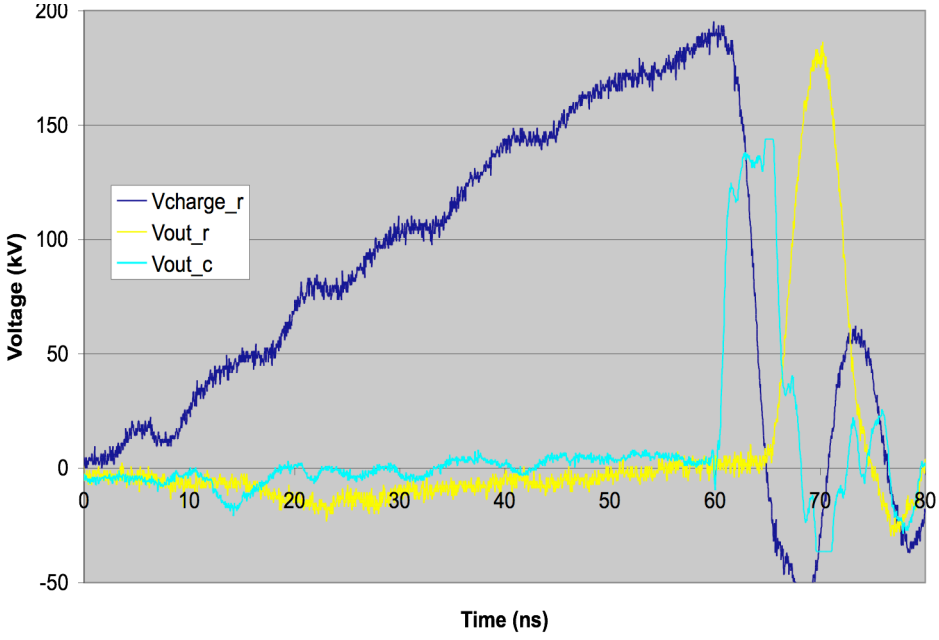
200
150
100
50
0
-50
Voltage (kV)
0
10
20
30
40
50
60
70
80
Time (ns)
Vcharge_r
Vout_r
Vout_c

Fig. 8.

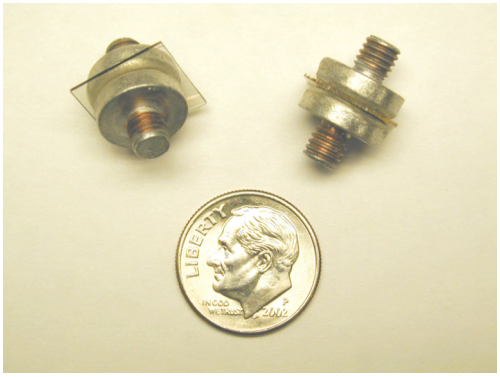
LIBERTY

Fig. 9.

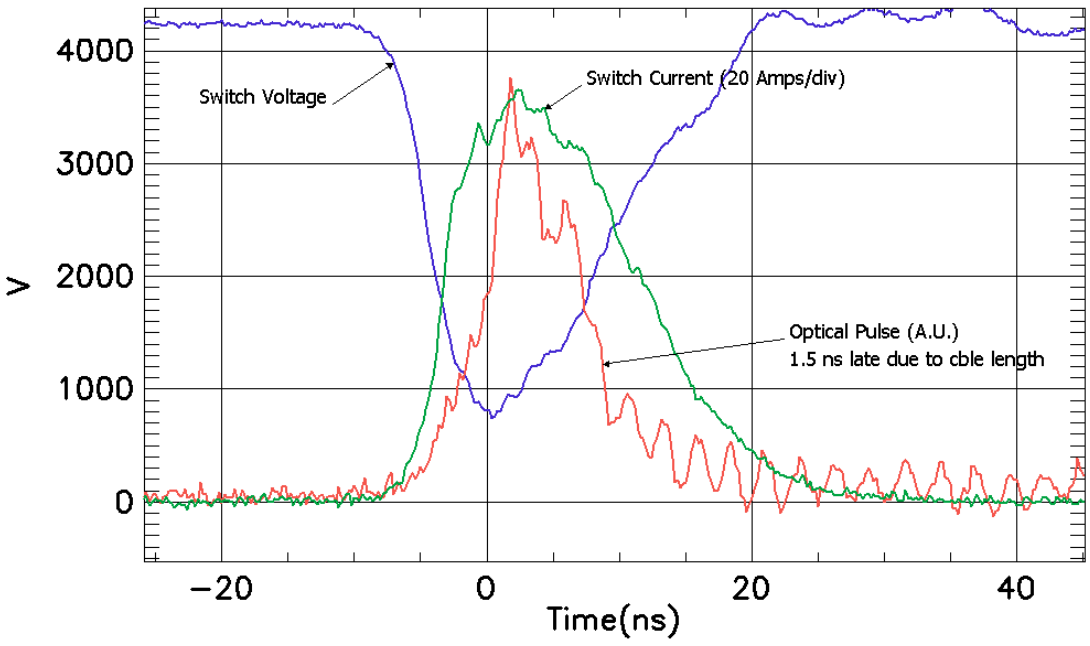
4000
3000
2000
1000
0
V
Switch Voltage
Switch Current (20 Amps/div)
Optical Pulse (A.U.)
1.5 ns late due to cble length
−20
0
20
40
Time(ns)

Fig. 10.

Fig. 11.

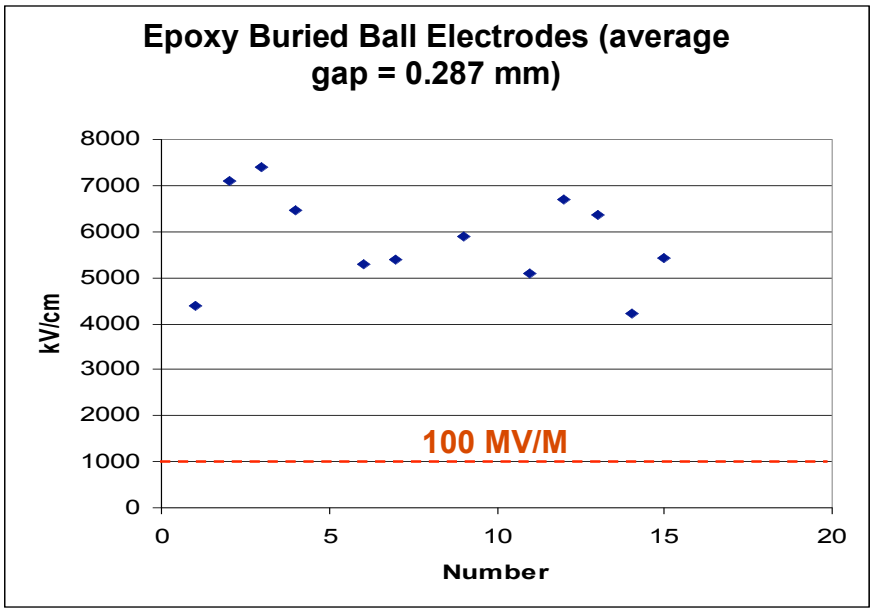
Epoxy Buried Ball Electrodes (average gap = 0.287 mm)
8000
7000
6000
5000
4000
3000
2000
1000
0
kV/cm
100 MV/M
0
5
10
15
20
Number

Fig. 12.

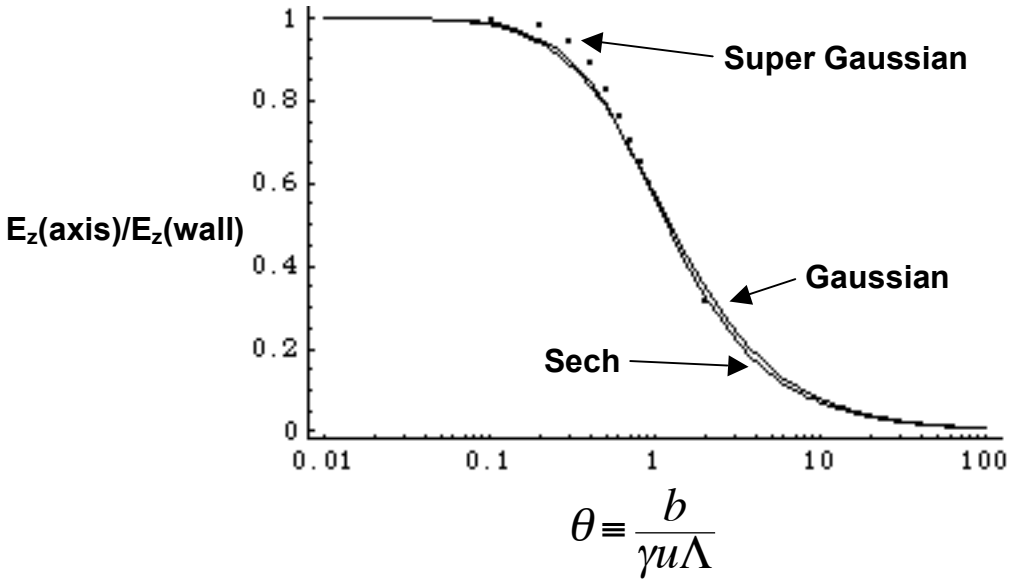
Super Gaussian
Gaussian
Sech
E_z(axis)/E_z(wall)
1
0.8
0.6
0.4
0.2
0
0.01
0.1
1
10
100
$\theta \equiv \frac{b}{\gamma u \Lambda}$

Fig. 13.

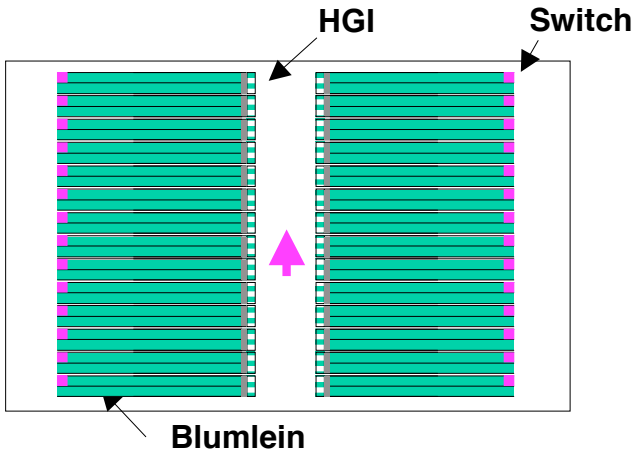
HGI
Switch
Blumlein

Fig. 14.

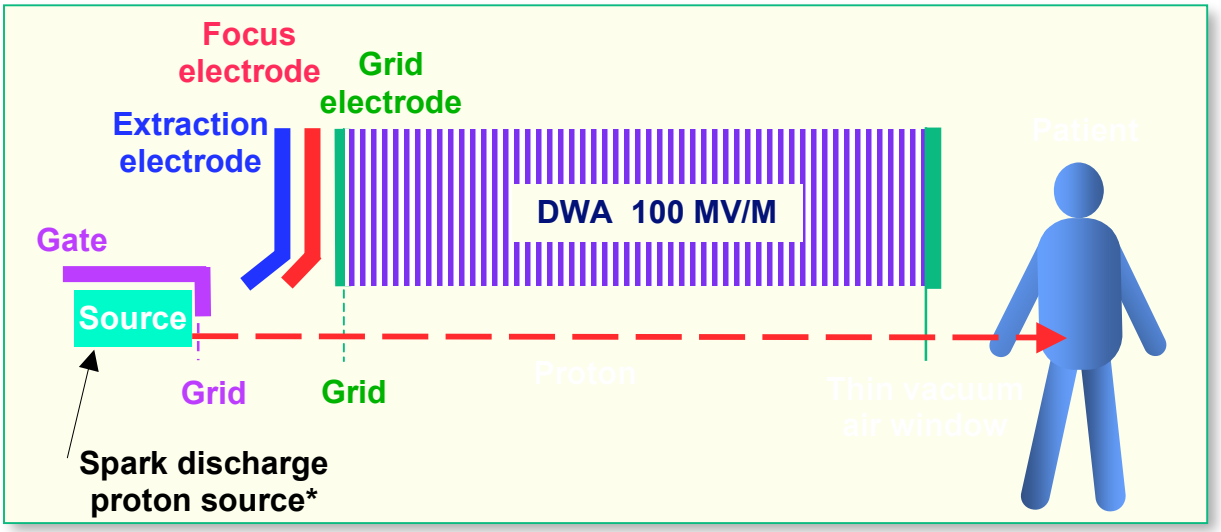
Focus electrode
Grid electrode
Extraction electrode
DWA 100 MV/M
Patient
Gate
Source
Grid
Grid
Proton
Thin vacuum air window
Spark discharge proton source*

Fig. 15.

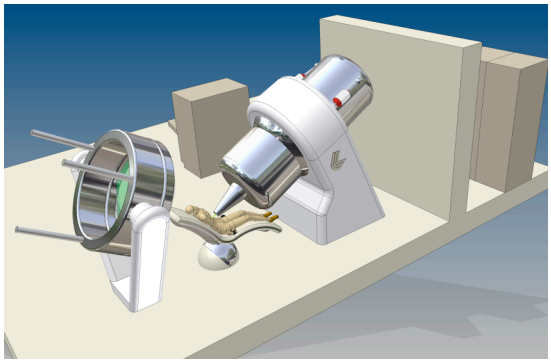

1

2

3 Fig. 16.

4